ARMY RESEARCH LABORATORY


# Fiber Segment–Based Degradation Methods for a Finite Element–Informed Structural Brain Network

by P. Justin McKee, Amy M. Dagro, Manuel M. Vindiola, and Jean M. Vettel

ARL-TR-6739 November 2013

## NOTICES

### Disclaimers

The findings in this report are not to be construed as an official Department of the Army position unless so designated by other authorized documents.

Citation of manufacturer's or trade names does not constitute an official endorsement or approval of the use thereof.

Destroy this report when it is no longer needed. Do not return it to the originator.

**Army Research Laboratory**
Aberdeen Proving Ground, MD 21005-5069

**ARL-TR-6739** **November 2013**

# Fiber Segment–Based Degradation Methods for a Finite Element–Informed Structural Brain Network

**P. Justin McKee and Amy M. Dagro**
**Weapons and Materials Research Directorate, ARL**

**Manuel M. Vindiola**
**Computational and Information Sciences Directorate, ARL**

**Jean M. Vettel**
**Human Research and Engineering Directorate, ARL**

| REPORT DOCUMENTATION PAGE | Form Approved OMB No. 0704-0188 |
|---|---|



| 1. REPORT DATE *(DD-MM-YYYY)* | 2. REPORT TYPE | 3. DATES COVERED (From - To) |
|---|---|---|
| November 2013 | Final | May 2011–June 2013 |

**4. TITLE AND SUBTITLE**
Fiber Segment–Based Degradation Methods for a Finite Element–Informed Structural Brain Network

**5a. CONTRACT NUMBER**

**5b. GRANT NUMBER**

**5c. PROGRAM ELEMENT NUMBER**

**6. AUTHOR(S)**
P. Justin McKee, Amy M. Dagro, Manuel M. Vindiola, and Jean M. Vettel

**5d. PROJECT NUMBER**

**5e. TASK NUMBER**

**5f. WORK UNIT NUMBER**

**7. PERFORMING ORGANIZATION NAME(S) AND ADDRESS(ES)**
U.S. Army Research Laboratory
ATTN: RDRL-WMP-B
Aberdeen Proving Ground, MD 21005-5069

**8. PERFORMING ORGANIZATION REPORT NUMBER**
ARL-TR-6739

**9. SPONSORING/MONITORING AGENCY NAME(S) AND ADDRESS(ES)**

**10. SPONSOR/MONITOR'S ACRONYM(S)**

**11. SPONSOR/MONITOR'S REPORT NUMBER(S)**

**12. DISTRIBUTION/AVAILABILITY STATEMENT**
Approved for public release; distribution is unlimited.

**13. SUPPLEMENTARY NOTES**

**14. ABSTRACT**
Through our research we aim to understand how a traumatic brain insult damages the brain's structural network that enables functional communication between brain regions. This report presents an expansion of our previous methods used to create a finite element–informed structural network model of the human brain by introducing a new method for network degradation. Tractography fibers from diffusion-weighted imaging contribute to the material properties of white matter. These fibers also constitute the undamaged structural network in the model. Unlike our previous work, only fiber segments within areas of high damage based on local tissue formations are removed. The resulting structural damage from two blast-loading conditions is successfully differentiated and quantified using standard graph property metrics from network science. Furthermore, we extend our previous work by examining whether these properties are scale-invariant by looking at a 12-node network as well as larger networks. Methods developed here allow for future work that will couple the degraded structural network with a separate neurophysical model to study how structural damage manifests in changes to the electrical oscillations of a functional brain network.

**15. SUBJECT TERMS**
traumatic brain injury, structure-function coupling, finite element method, structural brain network, blast simulation

| 16. SECURITY CLASSIFICATION OF: | | | 17. LIMITATION OF ABSTRACT | 18. NUMBER OF PAGES | 19a. NAME OF RESPONSIBLE PERSON |
|---|---|---|---|---|---|
| a. REPORT | b. ABSTRACT | c. THIS PAGE | | | P. Justin McKee |
| Unclassified | Unclassified | Unclassified | UU | 34 | 19b. TELEPHONE NUMBER (*Include area code*) 410-278-3031 |

**Standard Form 298 (Rev. 8/98)**
Prescribed by ANSI Std. Z39.18

## Contents

## List of Figures



## List of Tables

## Acknowledgments

We would like to thank the following individuals:

- Reuben Kraft, Kaleb McDowell, Peter Chung, and Piotr Franaszczuk for their involvement in the creation and/or execution of the Director's Strategic Initiative that developed the research program for the technical work described in this report.
- Adam Sokolow and Alfred Yu for their assistance with editing this report.

INTENTIONALLY LEFT BLANK.

# 1. Introduction

Assessment, delineation, and treatment of traumatic brain injury (TBI) are critically needed across civilian and military populations. The national cost of TBI is estimated to be $60 billion annually, with 3.2 million Americans living with disabilities due to TBI (*1*). Blast-related TBI is of particular interest due to its prevalence in recent military conflicts (*2*). Blast exposure results in a complex loading that presents many possible mechanisms of injury. Diffuse axonal injury is one particular injury mechanism that has been cited as a predominant signature injury of TBI neural damage (*2, 3*). This injury is characterized by widespread structural lesions in white-matter fiber tracts, the axons of neurons. These tracts connect brain regions into a structural network and allow neurons to communicate with one another (*4*, *5*). Degraded structural connectivity has been linked to disease states (*6, 7*), and it may underlie the cognitive deficits characteristic of mild, moderate, and severe cases of TBI (*8*). This report presents a multidisciplinary modeling effort that aims to improve our understanding of how mechanical loading to the head is related to changes in the structural network of the brain.

This modeling effort sits within a larger research program at the U.S. Army Research Laboratory (ARL) to understand brain structure-function couplings. The overall goal of this effort is to better understand how variability in structural connectivity due to traumatic insult or natural variability between healthy individuals relates to differences in the brain's functional connectivity (*9*, *10*) and, ultimately, to individual differences in human behavior. The modeling effort described here focuses on understanding the effects of traumatic brain insult. The use of a finite element (FE) simulation to degrade the structural brain network was first described in Kraft et al. (*11*). This report aims to make improvements to the structural network weighting and degradation methods. We examine if the graph metrics properties used to characterize the damaged structural network are scale-invariant to show damage consistently across different-sized networks. These improvements are needed to enable future research efforts that will couple the simulated structurally damaged network with a more coarse-grained electrophysiological model developed by David and Friston (*12*) and implemented at ARL (*9*, *13*, *14*). The electrophysiological model simulates functional electrical oscillations for a simulated brain region (node) in a defined structural network. The neural mass at each node represents a small patch of the brain containing several thousand interconnected neurons. Our research effort provides a unique capability to examine how functional ramifications (e.g., abnormal electrical oscillations between brain regions) are tied to parameters of blast-induced traumatic brain insults by using the damaged structural network from an FE simulation as input in the neurophysiological modeling. The long-term vision is to link how changes in these electrical oscillations interfere with functional connectivity patterns that are characteristic of successful performance on behavioral tasks

(*15–20*). Thus, the integration of two modeling efforts with ongoing experimental efforts provide a technical framework to investigate the well-known but poorly understood cognitive impairments that often result from traumatic brain insults (*9, 10*).

The modeling research described in this report makes use of concepts from structural FE analysis, structural neuroimaging methodologies, and graph theory analysis approaches from network science. In short, these tools are combined to improve the simulated mechanical response of brain tissue, estimate resulting damage to the structural connectivity in the brain, and develop graph-theoretic analysis approaches to quantify the resulting changes in the structural network. The methods described incorporate biological thresholds for brain tissue damage that are used to degrade the brain's structural connections and compute a resulting damaged structural network.

The FE method enables a physics-based computational simulation of a mechanical loading. The strength of this method is that it provides the full three-dimensional mechanical response of a material in time, thus providing insight into stress and strain that might not be possible to measure in vivo. Finite element simulations have been performed for both impact (*21–29*) and blast loading (*30–32*) to capture the mechanical response of the human head and brain. However, these investigations do not directly incorporate their results into plausible models of injury on a network level. The approach to link physics-based mechanical parameters and biological injury is an open research question. Our innovation is the combination of the FE method with neuroimaging to incorporate biological information into the model and improve mechanical response estimates and biological fidelity of cellular injury estimate.

A structural neuroimaging method, known as diffusion-weighted imaging, allows in vivo imaging of white-matter fiber tracts that are widely implicated in long-distance communication in the brain. This technique uses a magnetic resonance imaging (MRI) scanner to image the diffusion of water in the brain. This directional movement reveals the local brain structure since water diffuses in the same direction as the local fiber tract. Postprocessing, reconstruction tractography algorithms then estimate an individual's whole-brain fiber tract structure. These fiber tracts constitute the structural network of the brain. It is possible to then characterize this network using analytic approaches from network science.

Graph theory analysis methods from network science quantify topological properties of networks, and they have been successfully adopted for characterization of brain connectivity (*33*). The brain is divided into smaller regions of interest (ROIs) to provide graph nodes, and the white-matter connections between the ROIs provide the graph edges. Standard measures of graph properties can then be computed to characterize the structural brain network. We focus on seven key measures in our analysis: degree, shortest path, efficiency, betweenness, clustering coefficient, modularity, and assortivity. The degree measure is computed for each node, which is the sum of edge weights connected to a node. A short path in the network is the number of edges

traversed or the sum of weights along the most direct route from one node to another. Efficiency can be calculated as a nodal measure referred to as local efficiency, or for the network as a whole as global efficiency. This value represents how well connected the network is compared with a perfectly connected network (*34*) and captures the networks capacity for communication along short paths (*35*). Betweenness is the number of times a node is part of the shortest path between two other nodes (*34*). A high measure of betweenness is an indication of a hub used to allow efficient long-distance communication of nodes (*34*). The clustering coefficient is a measure of how well a particular node and its neighbors are connected to each other (*34*). Modularity is a value that can indicate the presence of a community structure composed of localized clusters of nodes (*36*). The assortativity quantifies how similar nodes are to each other in terms of their degree (*34*).

The graph theoretic framework has been applied to examine effects of lesions on network models of the brain. Several groups have investigated the effects of lesions on network models of the brain in both animal models (*37*, *38*) and humans (*7*, *39*). Young et al. (*37*) provide an early example of applying damage to a structure-function coupled network based on the thalamocortical system of a cat. They use anatomical data to create a weighted structural network and simulate the functional network. A lesion is simulated by removing a node from the network to show that there are functional effects that extend beyond the lesion site (*37*). Alstott et al. (*39*) extend this concept to the human brain by using diffusion-weighted imaging to create a whole brain structural network. They show that specific structural network measures, such as betweenness and efficiency, can characterize the network and quantify the effect of removing nodes. These research efforts establish the use of networks to describe the brain as a whole as well as with simulated lesions. Our work will complement these efforts by developing injury models that degrade the network to represent specific loading conditions.

We present a combination of the FE method with neuroimaging and network modeling to incorporate biological information into the model and provide the capability to evaluate the global effect of specific blast loading conditions. The work presented in this report represents several accomplishments that expand on previous work (*11*). In this work we discuss the edge-weighting method and how it is modified to make use of tractography fiber segments rather than whole fibers. This prevents the complete removal of edges from the structural network seen in previous work. Sensitivity of the network is then evaluated by comparing two simulations that represent a frontal blast loading and a blast loading from the side to show the ability to differentiate between these loading directions. Finally, the effect of scaling the number of ROIs in the structural network is investigated. An evaluation of network measures is performed to determine which are scale-invariant between networks of different sizes after damage is applied.

## 2. Methods

We briefly summarize some of our methods of this research and organize them as follows. Section 2.1 describes the procedure used to create the FE mesh from neuroimaging data. Section 2.2 provides detail of the FE model, including the loading conditions, material properties, and results of the simulation. Section 2.3 shows how FE results are formatted for use with the structural network and brain atlas. In section 2.4, we introduce our new fiber segment network degradation method and discuss how it is different from Kraft et al. (*11*).

### 2.1 Neuroimaging and FE Mesh Creation

Methods to create the FE model and reconstruct data from diffusion-weighted imaging are described in detail in Kraft et al. (*11*, *40*) and only summarized here. In short, geometry is created from MRI data by using the software Amira (*41*) to segment the head into white matter, gray matter, cerebrospinal fluid, skull, skin, and other soft tissue outside of the skull. In addition to the head, a torso from the Open 3D Project (*42*) is included to more accurately capture blast propagation to the brain. This geometry is used to generate a tetrahedral mesh for FE simulation. Tractography is reconstructed from a diffusion-weighted imaging technique called diffusion tensor imaging. This technique provides information of diffusion as a tensor value that can be used to reconstruct the fiber tractography (*43*).

### 2.2 FE Simulation

Here we briefly summarize some of the key features of the model; details of our material parameters and constitutive equations are described in detail in Kraft et al. (*11*, *40*). Tractography from diffusion tensor imaging data is incorporated into the three-dimensional FE model using a transverse isotropic material model specifically developed for representing white-matter tissue (*44*, *45*) where each FE is assigned an orientation based on the superimposed tractography (*40*). Material constitutive descriptions and properties for all components are described in detail in Kraft et al. (*11*). These material descriptions include properties for the skull, cortex, brain stem, cerebrospinal fluid, and soft tissue, which is an homogenized mixture of muscle and skin. The volume of the body is also modeled as an homogenous soft tissue to more accurately capture pressure loading that is transmitted to the head. A nodal-based tetrahedral formulation is used to resolve locking issues that are related to standard tetrahedral elements to better represent soft tissues (*46*).

The transient response of the blast loading to the head is simulated in Sierra (Sandia National Laboratories), an explicit FE method Lagrangian code. The blast-loading method combines the TNT air blast work of Kingery and Bulmash (*47*) and Randers-Pehrson and Bannister (*48*), with Sachs scaling to match the ConWep code (*49*). The code accounts for the angle of incidence by

transitioning from reflected to incident pressure by the relationship described in Gullerud et al. (*46*). For the comparison examined in this paper, two blast conditions are simulated. A frontal loading is simulated by a TNT spherical air-blast equivalent of 7.5 lb located 0.4 m above the ground and a 2-m standoff distance in the front. A side loading is simulated by a TNT spherical air-blast equivalent of 7.5 lb located 0.4 m above the ground and a 2-m standoff distance from the right of the body.

The results of the two loading conditions are presented in figure 1 as time history plots of the pressure, axonal strain, and strain-rate for the frontal loading (panels A–C) and side loading (panels D–F). Pressure is positive in compression. Axonal strain is defined as the strain in the direction of the axon based on the tractography within an element. Strain rate is an effective measurement based on the strain-rate tensor. These parameters have been used to predict cellular injury within neuronal cellular cultures (*50*). The five regions of interest plotted include the frontal lobe (red), temporal lobe (green), occipital lobe (blue), parietal lobe (orange), and corpus callosum (black). In both loading conditions, the blast wave produces a rapid rise in pressure at around 2 ms, which is qualitatively similar for all of the five regions (panels A and D).

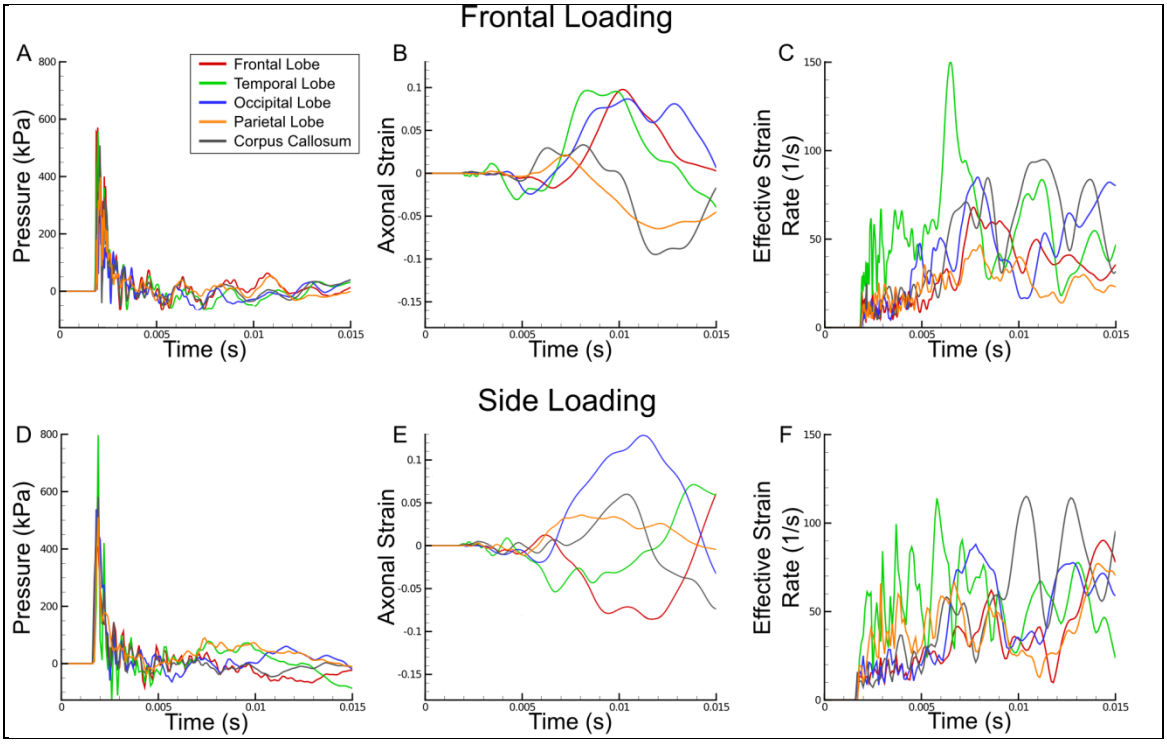


Figure 1. Finite element results. Pressure, axonal strain, and effective strain rate measured at various locations of the brain in both blast loading scenarios.

What follows the onset of the initial pressure wave are a number of smaller-amplitude and lower-frequency pressure waves that vary from region to region. Interestingly, the largest axonal strains (panels B and E) occur several milliseconds after the initial pressure wave. The large axonal strains are the result of the angular rotation of the head. This motion occurs more slowly than the pressure wave passing through the head, resulting in a delay before the axonal strain increases. The effective strain rate (panels C and F) shows high-frequency oscillations. Strain rate has been shown to contribute to cellular death in some brain regions (*51*) so it is important to consider this value along with the axonal strain. Emphasis should be placed on regions that show a high axonal strain and effective strain rate, such as the occipital and temporal lobes. These regions are more likely to show damage, and it will be shown that they have a higher network degradation.

The primary purpose of this work is to describe a new method for degradation of the structural network and evaluate its use on a small network for future use as input into a functional electrophysiological model. While the model presented in this work is currently not validated for blast loading conditions, these simulations provide two possible scenarios to compare the network response. This allows for the investigation of structural network degradation that results from tissue deformation calculated from an FE simulation. Validation of blast loading and a more detailed description of the mechanics involved in the blast simulation will be discussed in future work.

### 2.3 Mapping FE Data to Voxel Space

To make use of neuroimaging data, FE results are mapped to the standardized voxel space in magnetic resonance data, where each voxel represents a 2- × 2- × 2-mm cube of brain tissue. This mapping ensures that the FE data has the same volume, resolution, and Cartesian coordinates as the diffusion tensor data. This also allows the analysis to link with standardized brain atlas data that contains coordinates and labels for common brain regions studied in the neuroscience field (*52*). There are two possible qualifications where an element variable is assigned to a voxel as illustrated in figure 2. In this image, the black grid is a representation of voxels and the yellow triangles represent elements. Panel A shows a case where an element is assigned to voxels where the center of the voxel is contained within the element (red dots). Panel B shows an an element that does not contain any voxel centers. In this case, the element is assigned to the voxel that contains the element's centroid (blue dot). Multiple elements within a single voxel are averaged.

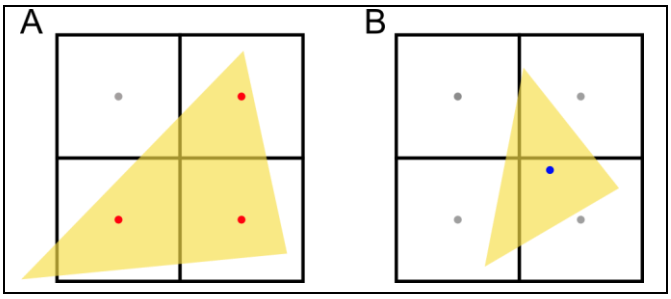


Figure 2. Element to voxel assignment.

### 2.4 Network Construction and Degradation

A damage parameter based on cellular death is then calculated for each voxel using an empirical formula for cellular death up to four days post-insult based on the assigned axonal strain and effective strain rate (*11*, *50*). This single-damage parameter is then used as a means to degrade the structural network. A cell death threshold for electrophysiological injury is estimated based on the work of Bain and Meaney (*53*), who claimed that electrophysiological injury would initially occur between 13% and 28% strain in a guinea pig optic nerve, and suggested an optimal threshold of 18% strain at a strain rate between 30 to 60 $s^{-1}$ (*53*). Applying these values to the equation for cellular death results in an average of 2.1% for injury initiation and 3.4% cell death for the optimal injury threshold for this range of strain rates. Using these cell death values is beneficial because it incorporates strain, strain rate, and time after injury into a single value that is used as a threshold for damage. This will help to account for the effects of high-rate loading and allow for a prediction of injury even at a lower strain if the strain rate is sufficient to allow the cell death to reach threshold values.

The Connectome Mapper Toolkit is used to parcellate the brain into 83 regions of interest as in previous work (*11*) based on the Desikan-Killiany brain atlas (*52*). The network is then resampled to 12 cortical ROIs to investigate methods to maximize compatibility with different size networks. These are the frontal lobe, parietal lobe, occipital lobe, medial temporal lobe, lateral temporal lobe, and cingulate cortex in both the left and right hemisphere. These 12 ROIs become the nodes of the network. Figure 3 shows the original 83-node parcellation from a lateral view A and medial view B where colors are used to separate the regions. The smaller cortical regions in each lobe are combined to form the new 12 ROIs. These new regions are shown in C and D for the lateral and medial view, respectively. There is the potential for variation in the resulting network measures when down-sampling to a 12-node because network measures are dependent on the topology of the network. Networks with 68, 114, 216, 446, and 1002 nodes are also created by subdividing the original parcellation using the process described by Cammoun et al. (*54*). This is done to better understand how this change in topology will affect network degradation.

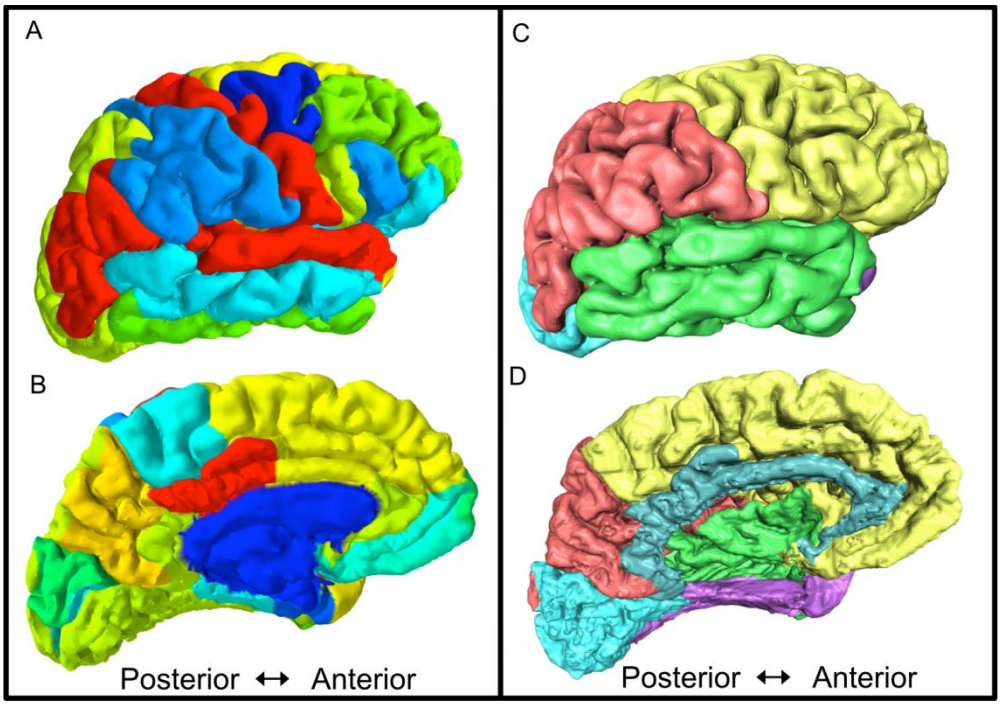


Figure 3. An illustration of the surface parcellation. The original 83-node parcellation shown from a lateral view (A) and medial view (B) is used to create a 12-node cortical parcellation shown from a lateral view (C) and medial view (D).

Fiber tractography from diffusion tensor imaging in combination with the ROIs created during the parcellation are used to create the initial network. Fibers that begin in one ROI and end in another represent a pathway for communication. This connection is represented by an edge between two nodes. Figure 4 illustrates a simplified picture where the grey represents ROIs and the black lines are tractography fibers that make up an edge between the two ROIs. The squares of the grid are a simplified two-dimensional illustration of voxels. Network edges are given weights to account for connection strength using a method that will be referred to as the fiber segment method. Each fiber is divided into segments based on the number of voxels that it passes through. The number in each voxel of figure 4 is the number of fiber segments contained within. The weight of an edge between two ROIs is equal to the total number of fiber segments in all tracts that connect these ROIs divided by the number of voxels on the edge. The example in figure 4A results in a weight of 2. This method is different from the weighting method in Kraft et al. (*11*), which weights edges based on the fiber as a whole. Panel B of figure 4 shows an example of a damaged connection. Voxels are weighted in red if they are above the minimum cellular death threshold. Numbers shown in red are the remaining fiber segments after damage is applied. The weighting of the edge is based on the number of fiber segments that remain after damage is applied. Dividing by the number of voxels in the edge accounts for long-distance connections that would be composed of a large number of fiber segments. Edge weights are

degraded by removing fiber segments from voxels that meet or exceed the cell death threshold. The percentage of fiber segments removed is 0% at or below the lower threshold of 2.1% cell death and increases linearly to 100% fiber segment removal at the upper threshold of 3.4% cell death.

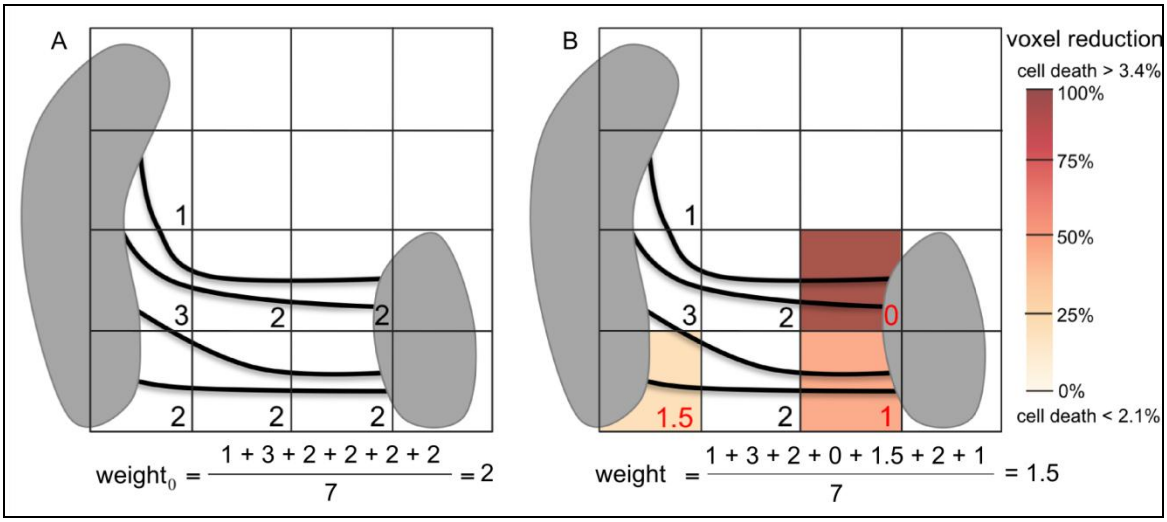


Figure 4. Fiber segment method edge degradation. An illustration of an example edge made up of two regions of interest connected by tractography fibers. (A) shows the edge before degradation and labels the number of fiber segments within each voxel. (B) shows an example of cell death data applied to degrade the edge.

Weights are resampled to a Gaussian distribution $N(.5.1^2)$ into the range [0,1]. This is based on procedures developed by Honey et al. (*55*), who stated the assumption that interregional physiological efficacies would not span the large range that is seen in the data before resampling. This Gaussian weight degradation is defined as $G = G_0 [W/W_0]$, where $G$ is the damaged Gaussian weight, $G_0$ is the undamaged Gaussian weight, $W$ is the damaged weight, and $W_0$ is the undamaged weight.

The fiber segment method is beneficial because it avoids the complete removal of edges seen in previous work by Kraft et al. (*11*). This method results in a lower estimation of network loss compared to previous methods where the entire fiber is removed but the pattern of degradation remains the same. However, there are several potential limitations of this weighting method. First is the assumption that fibers that pass through a region with a high damage value retain some capacity for communications. While this would not be valid for a single axon, it is reasonable in the case of a fiber segment representing the volume of a voxel at a resolution of 2 $mm^3$. This segment of fiber will be composed of a large number of axons, some of which may be damaged while others survive and can propagate an electrophysiological signal. Next, due to limited experimental data, this method cannot represent smaller-scale injury mechanisms and cannot provide a realistic quantitative value of axonal death. The use of a threshold limits the range of damage prediction to this value. This is useful because it allows for greater sensitivity

for detecting minor injury, but reductions in edge weight do not necessarily correspond to the same reduction in biological signaling capacity of cells that connect the ROIs. Despite these issues, this method is useful because it offers an estimate of the scale of damage. It is used to determine where damage occurs and the relative severity of the damage seen in different regions of the brain. This will be helpful for differentiating possible injury based on different loading conditions. This model will be improved to produce a more biologically accurate prediction of structural network damage as relevant experimental data becomes available.

## 3. Results and Discussion

### 3.1 Network Degradation

Figure 5 shows the fiber tractography for frontal loading in panels A–D and side loading in panels E–H for the 24-, 48-, 72-, and 96-h time points. The anterior direction is to the right and the posterior direction is to the left. Undamaged fibers are colored based on their direction, with green, blue, and red representing anterior-posterior, inferior-superior, and left-right, respectively. Fiber segments that are removed from the model are displayed in black. Relatively few fibers are removed in the frontal-loading condition until 72 h. At 96 h, the location of removed fibers is distributed throughout the volume of the brain. The side loading shows a high concentration of fiber segments that are removed in the occipital lobe starting at 48 h, which corresponds to the high strain and strain rate that is seen in the FE time-history plots in figure 6. The location of removed fibers continues to expand up to 96 h. This image format, developed by Alper et al. (*56*), displays the undamaged edge weight colored by edge strength overlapped with a smaller square that is colored by the damaged edge weight. Because this is an undirected network that produces a symmetrical matrix, the two halves are weighted to show different values. The blue-weighted half shows the edge strength and the red-weighted half shows the normalized edge strength. The regions of interest are the medial temporal, lateral temporal, frontal, parietal, occipital, and cingulate cortices in the right hemisphere for regions 1–6 and left hemisphere for regions 7–12.

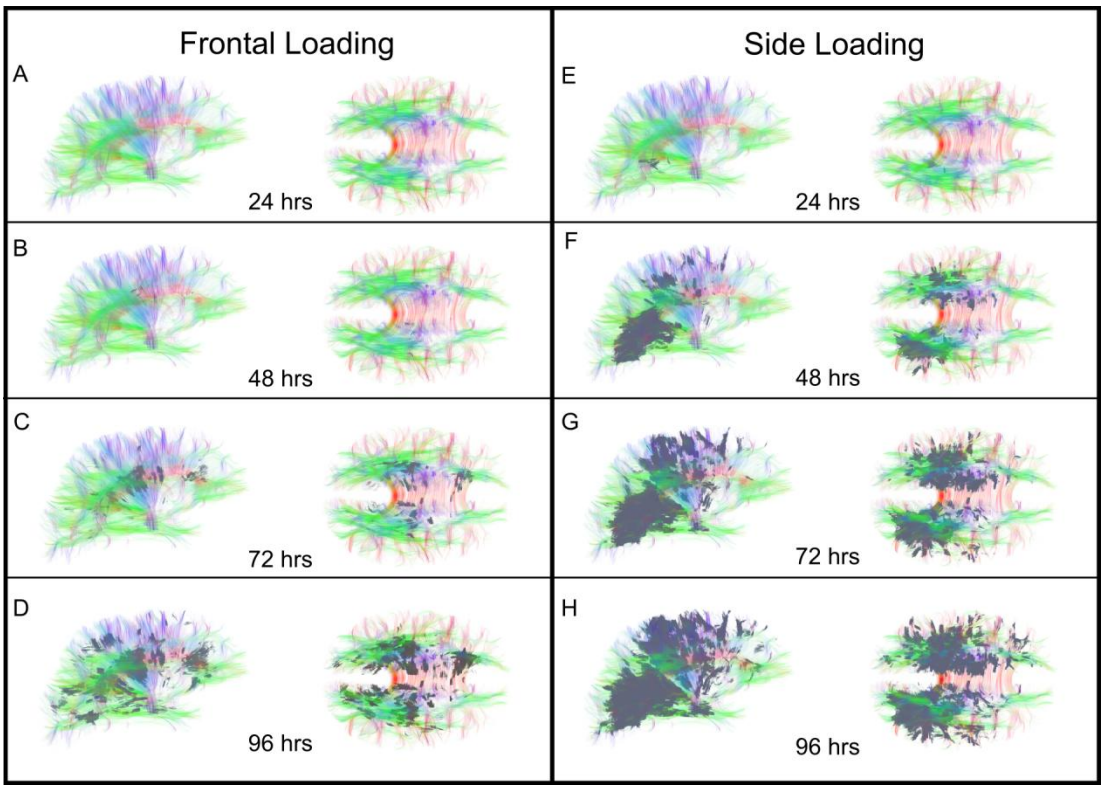


Figure 5. Evolution of fiber segment removal, using empirically based cellular death predictions obtained from in vitro models of neural tissues. Local strain and strain-rate values computed from FE simulations are used to specify injury.

Basic measurements are calculated from the data represented in figure 6. The weight at each edge of the network is represented by a single element of the matrix that corresponds to a connection between two specific ROIs. This is the most localized measure to investigate damage between two regions. The degree is calculated as the sum of matrix elements along a single column or row for any one node. This nodal measure shows damage to any one node based on all of its connections. The inner square of each matrix element represents the value at the current time point for comparison to the outer square that represents the initial value. The regions of interest are medial temporal, lateral temporal, frontal, parietal, occipital, and cingulate cortices in the right hemisphere for regions 1–6 and left hemisphere for regions 7–12. The red-weighted half of the matrix shows the normalized edge strength, and the sum of all edge weights is calculated by the sum of all matrix elements in the blue-weighted half of the matrix. This value provides a global account of the network to show how it has changed as a whole.

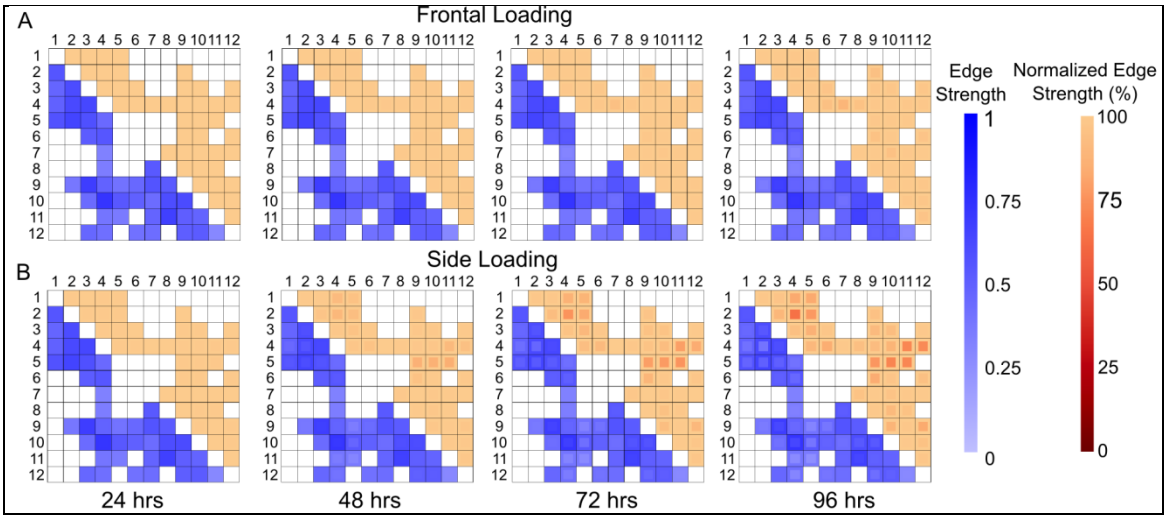


Figure 6. Undirected connectivity matrices.

The frontal-loading condition is shown in figure 6, panel A. This figure shows that there is little damage applied to the network on a global level with 1.8% reduction in the total edge strength at 96 h. Because of the subtle change in this global measure, it is important to consider localized measures of damage. Table 1 shows the percentage change in both degree and edge weight of the three most damaged regions or connections in either case.

Table 1. Percent change in degree and edge weight for the most damaged regions in the frontal-loading condition.

| **Region (No.)** | **Degree (%)** | **Edge Connection Number (No.)** | | **Weight Reduction (%)** |
|---|---|---|---|---|
| Cingulate R (6) | 3.4 | Parietal R (4) | Med. Temporal L (7) | 11.3 |
| Parietal R (4) | 2.6 | Lat. Temporal R (2) | Frontal L (9) | 5.7 |
| Cingulate L (12) | 2.3 | Parietal R (4) | Cingulate R (6) | 5.5 |

The side-loading condition is shown in figure 6 panel B. A larger global damage is seen in this case where the percent change in total edge strength is 10.3% at 96 h. Many connections show damage resulting in larger change in the degree and edge weight. These two measures are shown as a percentage change in table 2 for the most damaged regions or connections. While these results reconfirm that regions with high strain and strain rate seen in the FE results show higher network degradation, they also show damage to some additional ROIs. The right parietal lobe had low strain compared to other regions in the orange trace of figure 1, panel E.

However, the right parietal region is connected to other regions with high damage. As a result, the parietal lobe is at risk to be affected by damage to white-matter pathways from these distant brain regions.

Table 2. Percent change in degree and edge weight for the most damaged regions in the side-loading condition.

| Region (No.) | Degree (%) | Edge Connection (No.) | | Weight Reduction (%) |
|---|---|---|---|---|
| Occipital R (5) | 20.1 | Lat. Temporal R (2) | Parietal R (4) | 35.5 |
| Lat. Temporal R (2) | 16.4 | Occipital R (5) | Parietal L (10) | 28.4 |
| Parietal R (4) | 15.5 | Parietal R (4) | Occipital L (11) | 28.3 |

The betweenness indicates the presence of a hub in the network. This measure is calculated for the initial network to gain a better understanding of which ROI would potentially create a more widespread effect on the network if damaged. Figure 7 shows the betweenness for all regions. The highest values are seen in the parietal region in both hemispheres followed by the frontal lobe of both hemispheres. The right parietal region is among the top three most affected regions for degree in tables 1 and 2. This indicates that short paths traversing the parietal region may be especially disrupted as a result of damage to the structural network.

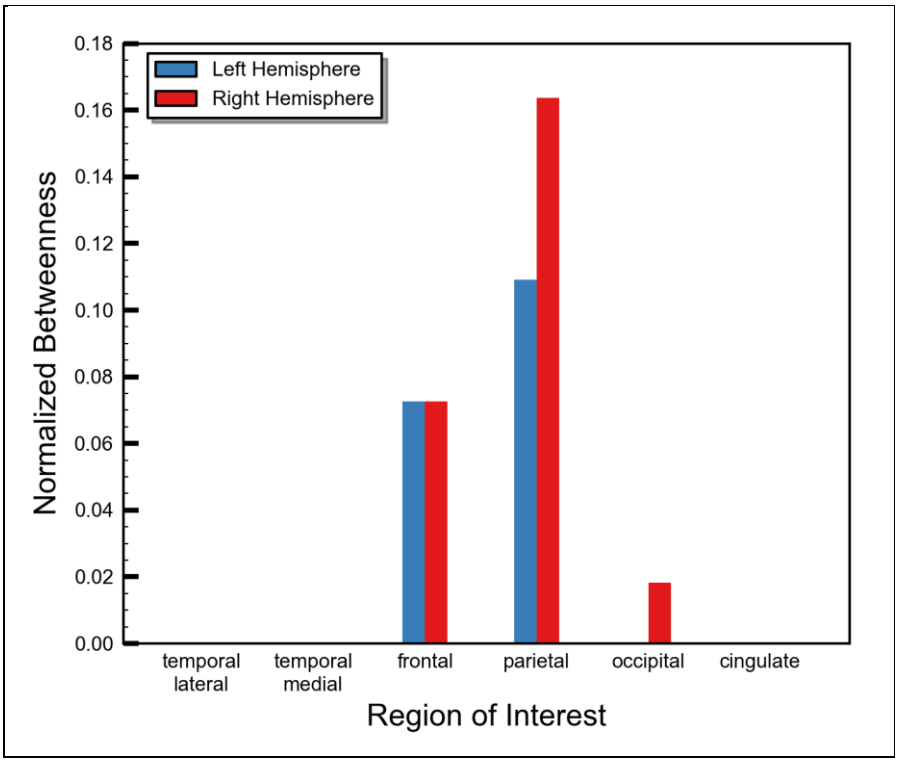


Figure 7. The betweenness value for each ROI. This plot shows that the parietal and frontal regions allow for the greatest number of multiedge connections along paths that minimize edge cost.

### 3.2 Network Measure Scale Invariance

An assessment of network measures is performed on 68-, 114-, 216-, 446-, and 1002-node cortical networks in addition to the 12-node network to better understand how the number of ROIs affects how damage is applied to the network. These additional networks are the result of subdividing the original parcellation (*54*). There is great variation in the value of network measures computed on the initial undamaged network at these different parcellation levels. This is shown for a selective representation of measures in figure 8, panels A–D. In panel A, the total edge strength of the network increases with the number of nodes because the networks composed of a larger number of nodes will have more edges. Both global efficiency and clustering coefficients (B and C) show significant change between 12 and 114 nodes. There is less variability in these values between 114 and 1002 nodes. The initial high values are the result of the 12-node network being the closest to a complete network where all regions are connected. The network topology is similar to a single cluster in the small networks rather than the collection of localized clusters that is seen in the larger networks. The efficiency and clustering coefficient are reduced as the network connections become more sparse after additional nodes are used to form the network. The increase in modularity in panel D at high parcellations indicates the formation of localized highly connected regions that are not present in the small networks.

It is important to consider normalized network measures due to the large variability of measures applied to networks of different scales. The normalized network measure is defined as $N = [M/M_0]\ 100\%$, where N is the normalized measure, M is the damaged measure and $M_0$ is the undamaged measure. By calculating this normalized measure, the amount of damage is more consistent across all parcellations. Panel E of figure 8 shows the normalized measure of total edge strength, global efficiency, clustering coefficient, average shortest path, assortativity, and modularity at 96 h. All networks shows similar normalized values of total edge strength, global efficiency, clustering coefficient, and average shortest path. Of these measures, the total edge strength in the side-loading condition has the greatest variation with at most 2.05% difference between networks with any number of nodes. However, modularity and assortativity show greater deviation at the 12-node network compared with other parcellations.

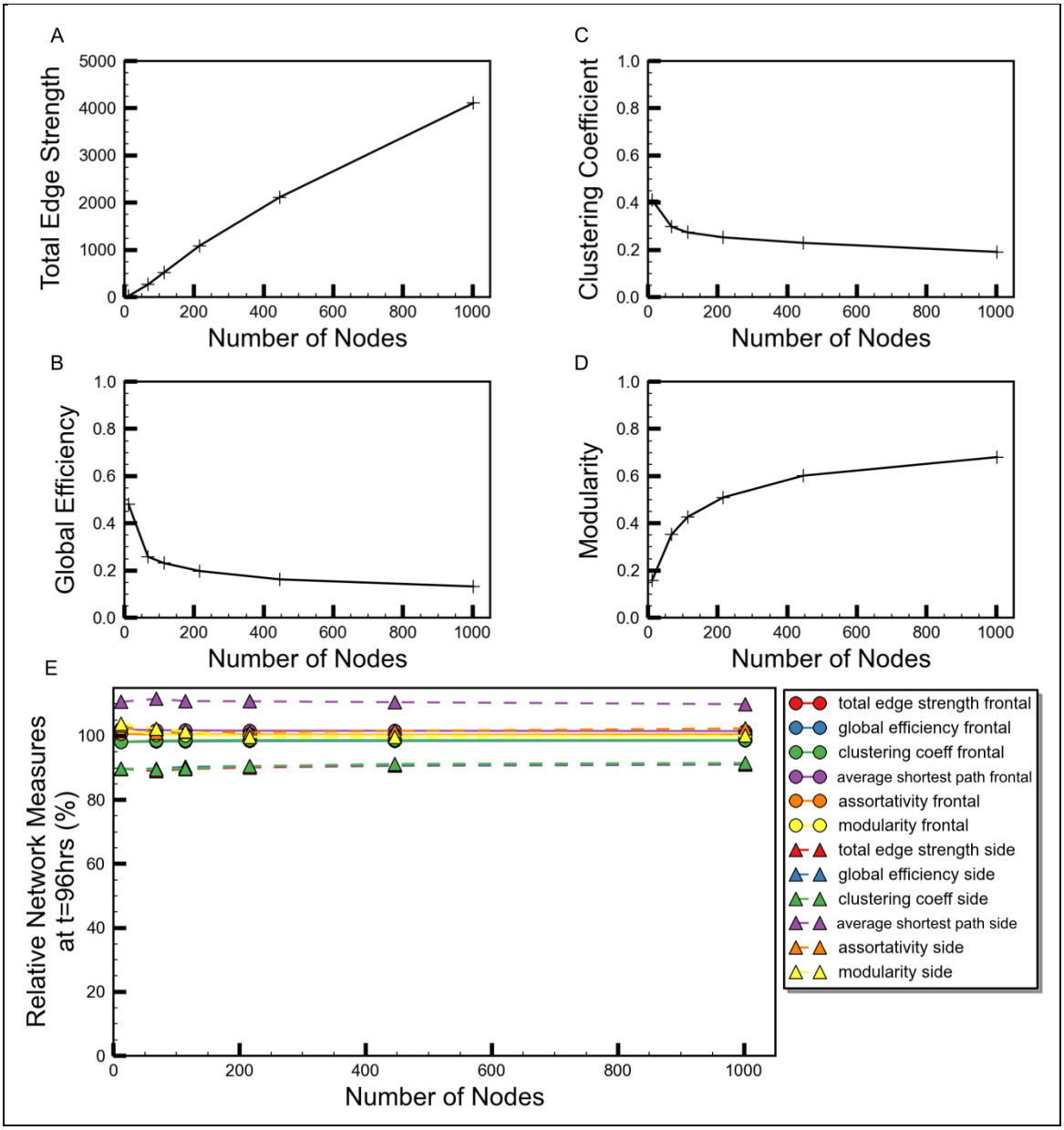


Figure 8. Effects of network scale.

### 3.3 Network Measure Sensitivity

In addition to being scale-invariant, a network measure should be sensitive to different loading conditions and be able to predict different magnitudes and locations of damage. Efficiency, clustering coefficient, and average shortest path maintain a consistent percentage of damage across all parcellations. These measures are chosen for a more detailed analysis of sensitivity. The efficiency is useful, as it can be calculated on a global and local scale. The ratio of average

clustering coefficient and average shortest path provides a measure that is comparable to the global efficiency (*35*). Figure 9 shows the relative total edge weight, efficiency, and ratio of average clustering coefficient and average shortest path through 96 h. The normalized values of these measures are 98.1%, 98.0%, and 96.1%, respectively, for the frontal loading and 89.7%, 89.6%, and 88.0%, respectively, for the side loading. All three measures are reduced consistently from 0 to 96 h. For the 12-node network and this level of damage, the more complex network measurements such as efficiency do not provide additional information.

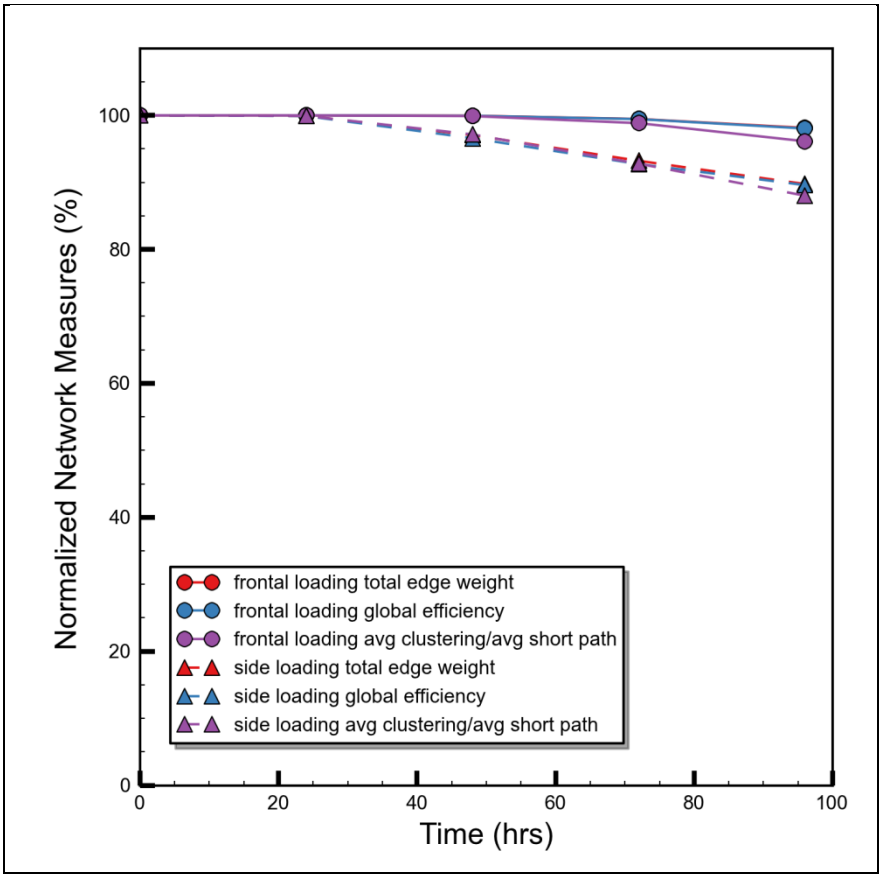


Figure 9. Normalized network measures. For this 12-node network, all measures show a similar trend. Note that side loading resulted in a larger change in these values.

An analysis of network measures is performed to compare the strength of connections between ROIs within the same hemisphere with connections that cross hemispheres to further differentiate between loading conditions. To do this, nodes are removed from one hemisphere to calculate the global efficiency of the remaining nodes. This results in a measure of global efficiency for the right hemisphere only and for the left hemisphere only. Figure 10 shows the normalized global efficiency for the right hemisphere, left hemisphere, and the whole brain for times up to 96 h. This shows that the normalized efficiency has a 9.0% difference in the right

hemisphere compared with the left hemisphere for the side-loading condition at 96 h. Note that the global efficiency of the brain as a whole in the right side-loading condition is reduced at a level similar to the right hemisphere. This indicates that the damage to edges that connect regions across hemispheres is great enough to cause more widespread effects. The frontal loading produces a more consistent reduction in normalized global efficiency for both hemispheres with only a 1.3% difference between the left and right. These results are expected based on the location of fiber segments removed. This shows that network measures are useful to quantify the difference in damage to the two hemispheres of the brain based on the loading.

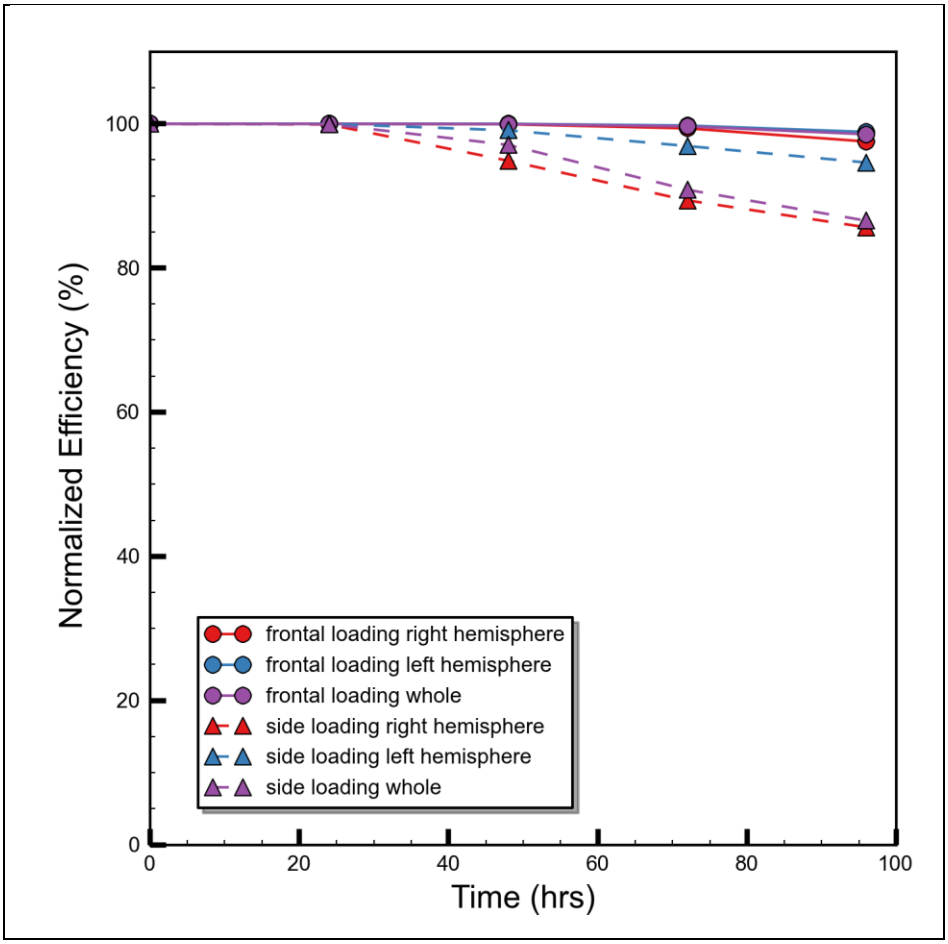


Figure 10. Lateral comparison of efficiency.

### 3.4 Discussion and Future Work

There are two key goals described in this research. The first is to evaluate the possibility of using a network with a low number of nodes by investigating which network measures are scale-invariant. Next is an assessment of the sensitivity of network measures for different loading conditions. The achievement of these two goals provides a better understanding of how the newly developed weighting methods produce damage in the structural network of the brain.

Results suggest that some graph measures are not scale-invariant. Topological information is distorted when down-sampling to a 12-node network. As a result, measures such as assortativity and modularity are not useful for this small-scale network. However, the normalized measure of damage is more consistent for the global efficiency, total edge weight, clustering coefficient, and average shortest path across networks with 12 to 1002 nodes. This shows that these network measures will be useful for comparing a network of any size.

Our results indicate that the new weighting method produces different patterns of damage to the structural network corresponding to the different loading conditions presented here. Network measures such as global efficiency, total edge weight, clustering coefficient, and average shortest path are used to show the difference in damage applied to the network on a global level. However, all of these measures predict a similar magnitude of global damage. On a 12-node network for these loading conditions, there is no advantage in using more complex network measures. This shows that local measures are necessary to understand the how damage is applied to the network. Nodes on the side closest to the blast origin were more damaged in the side-loading condition. However, there is only a small amount of variation in the degree in the front-loading condition. For this loading condition, individual edge weights are the most effective indication of where damage takes place. While this is a very simple measure, it is the most reliable estimation of damage for a small network such as the 12-node network investigated in this research. In addition, individual edge weights show the greatest sensitivity to minor damage when relatively few fiber segments are removed from the model. Because of this sensitivity, changes in individual edge weights are suggested for use to determine changes in coupling strength in an electrophysiological model.

In future work, the ability to make use of a functional brain network model based on a degraded structural network will allow for additional insight into the possible effects of blast loading to the brain. In the electrophysiological model, the simulated brain region nodes oscillate at particular intrinsic frequencies, and functional networks are formed by connections, or edges, between the nodes. The edge weighting in an electrophysiological model will be determined by the edge weights estimated in multiple degraded structural networks at different time points (e.g., undamaged and at 24, 48, 72, and 96 h). This will allow for the adjustment of coupling strength between simulated brain nodes to represent the functional aspect of the network, revealing how changes in edge weighting based on the loading condition manifests in changes in the functional brain network. Investigation of instability in the functional network due to simulated structural network damage predicated from an FE simulation can help improve not only our understanding of the physical damage to the brain but also the possibility of electrophysiological impairment. This provides a technical framework to use computational methods to understand how structural injury links to abnormal electrical oscillations that disrupt the functional connectivity patterns associated with successful task performance. In short, this framework links structural damage with disrupted functional connectivity that may underlie cognitive impairment.

## 4. Conclusions

Our larger research program on brain structure-function couplings at ARL integrates modeling and experimentation to elucidate the links among structural connectivity, functional connectivity, and behavioral performance. The research described in this report details a technical approach to improve the understanding of neurotrauma through the combined use of the finite element method, structural neuroimaging methods, and graph theory approaches from network science. This report presents an expansion of our previous methods using a physics-based simulation to inform structural brain network degradation. Our new weighting method using fiber tract segments provides increased sensitivity to structural network damage based on graded levels of cellular tissue damage. Our results indicate that the new weighting method can differentiate between loading conditions in the simulated damage to the structural network model. The results also indicate that some graph measures are not scale-invariant and should be selected based on the size of the network. Evaluation of a 12-node network shows that the most reliable measure of degradation is a reduction in individual edge weights.

Future work will use time-evolving estimates of degraded edge weights to inform the connections between simulated brain nodes in an electrophysiological model and examine how different blast-loading conditions change electrical activity in a functional brain network. By understanding which brain regions see diminished capacity for communication in the structural network, it may be possible understand instabilities in functional connectivity that may underlie the cognitive deficits characteristic of traumatic brain injuries. Substantial experimental work is needed to better understand how to relate the network degradation described in this work to biological injury. However, this method provides a preliminary pathway to construct more realistic models of mechanical tissue deformation using information about white-matter tracts from diffusion tensor imaging and to develop tools to understand how structural injury translates to functional network changes.

## 5. References


1. Pascrell House Home Page. Congressional Brain Injury Task Force. http://pascrell.house.gov/work/braininjury.shtml (accessed August 2013).

2. Gupta, R. K.; Przekwas, A. Mathematical Models of Blast-Induced TBI: Current Status, Challenges, and Prospects. *Frontiers in Neurology* **2013**, *4*, 59.

3. Taber, K.; Warden, D.; Hurley, R. Blast-Related Traumatic Brain Injury: What Is Known? *The Journal of Neuropsychiatry and Clinical Neurosciences* **2006**, *18* (2), 141–145.

4. Alivisatos, A. P.; Chun, M.; Church, G. M.; Greenspan, R. J.; Roukes, M. L.; Yuste, R. The Brain Activity Map Project and the Challenge of Functional Connectomics. *Neuron* **2012**, *74* (6), 970–974.

5. He, B.; Yang, L.; Wilke, C.; Yuan, H. Electrophysiological Imaging of Brain Activity and Connectivity – Challenges and Opportunities. *IEEE Transactions on Biomedical Engineering* **2011**, *58* (7), 1918–1931.

6. Bassett, D. S.; Bullmore, E.; Verchinski, B. A.; Mattay, V. S.; Weinberger, D. R.; Meyer-Lindenberg, A. Hierarchical Organization of Human Cortical Networks in Health and Schizophrenia. *The Journal of Neuroscience* **2008**, *28* (37), 9239–9248.

7. He, Y.; Wang, J.; Wang, L.; Chen, Z.; Yan, C.; Yang, H.; Tang, H.; Zhu, C.; Gong, Q.; Zang, Y.; Evans, A. Uncovering Intrinsic Modular Organization of Spontaneous Brain Activity in Humans. *PLoS One* **2009**, *4* (4), e5226.

8. Vettel, J. M.; Bassett, D.; Kraft, R.; Grafton, S. *Physics-Based Models of Brain Structure Connectivity Informed by Diffusion-Weighted Imaging*; ARL-RP-0355; U.S. Army Research Laboratory: Aberdeen Proving Ground, MD, 2010.

9. Vettel, J.; Dagro, A.; Gordon, S.; Kerick, S.; Kraft, R.; Luo, S.; Rawal, S.; Vindiola, M.; McDowell, K. *Brain Structure-Function Couplings (FY11)*; ARL-TR-5893; U.S. Army Research Laboratory: Aberdeen Proving Ground, MD, January 2012.

10. Vettel, J.; Vindiola, M.; Dagro, A.; McKee, P.; Kraft, R.; McDowell, K.; Franaszczuk, P. *Brain Structure-Function Couplings: Year 2 Accomplishments and Programmatic Plans*; ARL-SR-0268; U.S. Army Research Laboratory: Aberdeen Proving Ground, MD, June 2013.

11. Kraft, R.; Mckee, P.; Dagro, A.; Grafton, S. Combining the Finite Element Method With Structural Connectome-Based Analysis for Modeling Neurotrauma: Connectome Neurotrauma Mechanics. *PLoS Computational Biology* **2012**, *8* (8), e1002619.

12. David, O.; Friston, K. J. A Neural Mass Model for MEG/EEG: Coupling and Neuronal Dynamics. *NeuroImage* **2003**, *20* (3), 1743–1755.

13. Gordon, S.; Franaszczuk, P.; Hairston, W.; Vindiola, M.; McDowell, K. Comparing Parametric and Nonparametric Methods for Detecting Phase Synchronization in EEG. *Journal of Neuroscience Methods* **2013**, *212* (2), 247–258.

14. Vindiola, M.; Vettel, J.; Gordon, S.; Franaszczuk, P.; McDowell, K. Applying EEG Phase Synchronization Measures to Non-Linearly Coupled Neural Mass Models. Submitted to *Journal of Neuroscience Methods*, 2013.

15. Sakkalis, V. Review of Advanced Techniques for the Estimation of Brain Connectivity Measured With EEG/MEG. *Computers in Biology and Medicine* **2011**, *41* (12), 1110–1117.

16. Blinowska, K. J.; Kamiński, M.; Brzezicka, A.; Kamiński, J. Application of Directed Transfer Function and Network Formalism for the Assessment of Functional Connectivity in Working Memory Task. *Philosophical Transactions of the Royal Society A: Mathematical, Physical and Engineering Sciences* **2013**, *371*, 1997.

17. Ioannides, A. A.; Dimitriadis, S. I.; Saridis, G. A.; Voultsidou, M.; Poghosyan, V.; Liu, L.; Laskaris, N. A. Source Space Analysis of Event-Related Dynamic Reorganization of Brain Networks. *Computational and Mathematical Methods in Medicine* **2012**, 452503.

18. Philiastides, M. G.; Sajda, P. Causal Influences in the Human Brain During Face Discrimination: A Short-Window Directed Transfer Function Approach. *IEEE Transactions on Biomedical Engineering* **2006**, *53* (12), 2602–2605.

19. Supp, G. G.; Schlögl, A.; Fiebach, C. J.; Gunter, T. C.; Vigliocco, G.; Pfurtscheller, G.; Petsche, H. Short Communications: Semantic Memory Retrieval: Cortical Couplings in Object Recognition in the N400 Window. *European Journal of Neuroscience* **2005**, *21* (4), 1139–1143.

20. Sun, Y.; Zhang, H.; Feng, T.; Qiu, Y.; Zhu, Y.; Tong, S. Early Cortical Connective Network Relating to Audiovisual Stimulation by Partial Directed Coherence Analysis. *IEEE Transactions on Biomedical Engineering* **2009**, *56* (11), 2721–2724.

21. Horgan, T. J.; Gilchrist, M. D. The Creation of Three-Dimensional Finite Element Models for Simulating Head Impact Biomechanics. *International Journal of Crash Worthiness* **2003**, *8* (4), 353–366.

22. Takhounts, E.; Eppinger, R.; Campbell, J.; Tannous, R.; Power, E.; Shook, L. On the Development of the Simon Finite Element Head Model. *Stapp Car Crash Journal* **2003**, *47*, 107–133.

23. Sayed, T. E.; Mota, A.; Fraternali, F.; Ortiz, M. Biomechanics of Traumatic Brain Injury. *Computer Methods in Applied Mechanics and Engineering* **2008**, *197* (51), 4692–4701.

24. Ho, J.; Kleiven, S. Can Sulci Protect the Brain From Traumatic Injury? *Journal of Biomechanics* **2009**, *42* (13), 2074–2080.

25. Moss, W. C.; King, M. J.; Blackman, E. G. Skull Flexure From Blast Waves: A Mechanism for Brain Injury With Implications for Helmet Design. *Phys. Rev. Lett*. **2009**, *103*, 108702.

26. Moore, D. F.; Jérusalem, A.; Nyein, M.; Noels, L.; Jaffee, M. S.; Radovitzky, R. A. Computational Biology Modeling of Primary Blast Effects on the Central Nervous System. *NeuroImage* **2009**, *47*, T10–T20.

27. Nyein, M. K.; Jason, A. M.; Yu, L.; Pita, C. M.; Joannopoulos, J. D.; Moore, D. F.; Radovitzky, R. A. In Silico Investigation of Intracranial Blast Mitigation With Relevance to Military Traumatic Brain Injury. *Proceedings of the National Academy of Sciences* **2010**, *107* (48), 20703–20708.

28. Wright, R.; Ramesh, K. An Axonal Strain Injury Criterion for Traumatic Brain Injury. *Biomechanics and Modeling in Mechanobiology* **2012**, *11*, 245–260.

29. Yang, K. H.; Mao, H.; Wagner, C.; Zhu, F.; Chou, C. C.; King, A. I. Modeling of the Brain for Injury Prevention. In *Neural Tissue Biomechanics*; Bilston, L. E., Ed.; Springer: Berlin, 2011; Vol. 3; pp 69–120.

30. Taylor, P.; Ford, C. Simulation of Blast-Induced Early-Time Intracranial Wave Physics Leading to Traumatic Brain Injury. *Journal of Biomechanical Engineering* **2009**, *131*, 061007.

31. Nyein, M.; Jason, A.; Yu, L.; Pita, C.; Joannopoulos, J.; Moore, D.; Radovitzky, R. In Silico Investigation of Intracranial Blast Mitigation With Relevance to Military Traumatic Brain Injury. *Proceedings of the National Academy of Sciences* **2010**, *107* (48), 20703–20708.

32. Chafi, M.; Karami, G.; Ziejewski, M. Biomechanical Assessment of Brain Dynamic Responses Due to Blast Pressure Waves. *Annals of Biomedical Engineering* **2010**, *38* (2), 490–504.

33. Bullmore, E.; Sporns, O. Complex Brain Networks: Graph Theoretical Analysis of Structural and Functional Systems. *Nature Reviews Neuroscience* **2009**, *10* (3), 186–198.

34. Rubinov, M.; Sporns, O. Complex Network Measures of Brain Connectivity: Uses and Interpretations. *NeuroImage* **2010**, *52* (3), 1059–1069.

35. Latora, V.; Marchiori, M. Efficient Behavior of Small-World Networks. *Phys. Rev. Lett.* **2001**, *87*, 198701.

36. Newman, M. E. Modularity and Community Structure in Networks. *Proceedings of the National Academy of Sciences* **2006**, *103* (23), 8577–8582.

37. Young, M.; Hilgetag, C.; Scannell, J. On Imputing Function to Structure From the Behavioural Effects of Brain Lesions. *Philosophical Transactions of the Royal Society of London. Series B: Biological Sciences* **2000**, *355* (1393), 147–161.

38. Honey, C.; Sporns, O.; Cammoun, L.; Gigandet, X.; Thiran, J.; Meuli, R.; Hagmann, P. Predicting Human Resting-State Functional Connectivity From Structural Connectivity. *Proceedings of the National Academy of Sciences* **2009**, *106* (6), 2035–2040.

39. Alstott, J.; Breakspear, M.; Hagmann, P.; Cammoun, L.; Sporns, O. Modeling the Impact of Lesions in the Human Brain. *PLoS Computational Biology* **2009**, *5* (6), e1000408.

40. Kraft, R.; Dagro, A. *Design and Implementation of a Numerical Technique to Inform Anisotropic Hyperelastic Finite Element Models Using Diffusion-Weighted Imaging*; ARL-TR-5796; U.S. Army Research Laboratory: Aberdeen Proving Ground, MD, 2011.

41. FEI Visualization Sciences Group Home Page. http://www.vsg3d.com/amira/overview (accessed August 2013).

42. Open 3d Project Home Page. http://www.open3dproject.org (accessed August 2013).

43. Hagmann, P. *From Diffusion MRI to Brain Connectomics*. Thesis, Lausanne: Ecole Polytechnique Fdrale de Lausanne (EPFL), 2005.

44. Arbogast, K. B.; Margulies, S. S. A Fiber-Reinforced Composite Model of the Viscoelastic Behavior of the Brainstem in Shear. *Journal of Biomechanics* **1999**, *32* (8), 865–870.

45. Prange, M. T.; Margulies, S. S. Regional, Directional, and Age-Dependent Properties of the Brain Undergoing Large Deformation. *Journal of Biomechanical Engineering* **2002**, *124*, 244–252.

46. Gullerud, A.; Carpenter, J.; Scherzinger, B. *Presto 4.20 Users Guide: Addendum for Shock Capabilities*; Sandia National Laboratory: Albuquerque, NM, 2011.

47. Kingery, C.; Bulmash, G. *Air Blast Parameters From TNT Spherical Air Burst and Hemispherical Surface Burst*; U.S. Army Ballistic Research Laboratories: Aberdeen Proving Ground, MD, 1984.

48. Randers-Pehrson, G.; Bannister, K. *Airblast Model for Dyna2d and 3d.*; ARL-TR-1310; U.S. Army Research Laboratory: Aberdeen Proving Ground, MD,1997.

49. Hyde, D. *Conwep Users Manual*; Instruction Report SL-88-1; U.S. Army Engineer Waterways Experiment Station: Vicksburg, MS, 1988.

50. Morrison, B.; Cullen, D. K.; LaPlaca, M. In Vitro Models for Biomechanical Studies of Neural Tissues. *Neural Tissue Biomechanics* **2011**, *3*, 247–285.

51. Elkin, B. S.; Morrison B., III. Region-Specific Tolerance Criteria for the Living Brain. *Stapp Car Crash J* **2007**, *51*, 127–138.

52. Desikan, R. S.; Sgonne, F.; Fischl, B.; Quinn, B. T.; Dickerson, B. C.; Blacker, D.; Buckner, R. L.; Dale, A. M.; Maguire, R. P.; Hyman, B. T.; Albert, M. S.; Killiany, R. J. An Automated Labeling System for Subdividing the Human Cerebral Cortex on MRI Scans Into Gyral Based Regions of Interest. *NeuroImage* **2006**, *31* (3), 968–980.

53. Bain, A.; Meaney, D. Tissue-Level Thresholds for Axonal Damage in an Experimental Model of Central Nervous System White Matter Injury. *Journal of Biomechanical Engineering* **2000**, *122* (6), 615–622.

54. Cammoun, L.; Gigandet, X.; Meskaldji, D.; Thiran, J. P.; Sporns, O.; Do, K. Q.; Maeder, P.; Meuli, R.; Hagmann, P. Mapping the Human Connectome at Multiple Scales With Diffusion Spectrum MRI. *Journal of Neuroscience Methods* **2012**, *203* (2), 386–397.

55. Honey, C. J.; Sporns, O.; Cammoun, L.; Gigandet, X.; Thiran, J. P.; Meuli, R.; Hagmann, P. Predicting Human Resting-State Functional Connectivity From Structural Connectivity. *Proceedings of the National Academy of Sciences* **2009**, *106* (6), 2035–2040.

56. Alper, B.; Bach, B.; Henry Riche, N.; Isenberg, T.; Fekete, J. D. Weighted Graph Comparison Techniques for Brain Connectivity Analysis. *Proceedings of the Special Interest Group on Computer-Human Interaction Conference on Human Factors in Computing Systems*, Paris, France, 27 April–2 May 2013.

| NO. OF COPIES | ORGANIZATION |
|---|---|
| 1 (PDF) | DEFENSE TECHNICAL INFORMATION CTR DTIC OCA |
| 1 (PDF) | DIRECTOR US ARMY RESEARCH LAB IMAL HRA |
| 1 (PDF) | DIRECTOR US ARMY RESEARCH LAB RDRL CIO LL |
| 1 (PDF) | GOVT PRINTG OFC A MALHOTRA |
| 1 (PDF) | RDRL WMP B J MCKEE |

INTENTIONALLY LEFT BLANK.